MATERIALS SCIENCE

Boosting contact sliding and wear protection via atomic intermixing and tailoring of nanoscale interfaces

Neeraj Dwivedi[1]*, Reuben J. Yeo[1,2], Chetna Dhand[3], Jared Risan[4], Richard Nay[4], Sudhiranjan Tripathy[5], Sukumar Rajauria[6], Mohammad S. M. Saifullah[5], Subramanian K. R. S. Sankaranarayanan[7], Hyunsoo Yang[1], Aaron Danner[1], Charanjit S. Bhatia[1]*

Friction and wear cause energy wastage and system failure. Usually, thicker overcoats serve to combat such tribological concerns, but in many contact sliding systems, their large thickness hinders active components of the systems, degrades functionality, and constitutes a major barrier for technological developments. While sub-10-nm overcoats are of key interest, traditional overcoats suffer from rapid wear and degradation at this thickness regime. Using an enhanced atomic intermixing approach, we develop a ~7- to 8-nm-thick carbon/silicon nitride (C/SiN_x) multilayer overcoat demonstrating extremely high wear resistance and low friction at all tribological length scales, yielding ~2 to 10 times better macroscale wear durability than previously reported thicker (~20 to 100 nm) overcoats on tape drive heads. We report the discovery of many fundamental parameters that govern contact sliding and reveal how tuning atomic intermixing at interfaces and varying carbon and SiN_x thicknesses strongly affect friction and wear, which are crucial for advancing numerous technologies.

INTRODUCTION

Wear and friction remain the two most critical and long-standing issues in moving mechanical systems/devices (MMSDs) at all length scales (*1*–*3*). High friction is undesirable because of the extra mechanical energy that has to be consumed to overcome it, leading to energy losses. It is estimated that about one-third of automobile fuel is used just to overcome the unwanted effects of high friction (*1*, *2*). This excessive use of fuels and energy wastage is deleterious toward the environment and human health and incurs huge economical losses in the long term. At the same time, material wear is also a critical concern because the rapid removal and degradation of material result in early failure of various systems/devices (*1*–*3*). Magnetic storage devices, such as read/write heads, recording media of tape drives (TDs) and hard disk drives, probes for atomic force microscopy (AFM), micro- and nano-electromechancial systems (MEMS and NEMS), and many engineering scale components are some examples of MMSDs that suffer immensely from the adverse effects of wear and friction (*1*–*19*). In general, from environmental, human health, and economical viewpoints, even a small fraction of friction and wear reduction is vital for energy savings and increasing the operational lifetime of systems.

Surface coatings have evolved over the years as an excellent route to modify friction and wear (*2*, *4*–*9*). With miniaturization and advancement of modern devices/systems, the thickness budget of surface coatings in many devices and systems is shrinking year by year (*4*–*6*, *8*–*15*). However, most of the commonly used overcoats are very thick (from a few tens to hundreds of nanometers) (*1*, *13*–*19*), provide insufficient wear durability in many rigorous tribological conditions (*13*–*19*), and hinder the intrinsic functionality of several practical systems and devices (*4*–*6*). For example, Erdemir *et al.* (*1*) used a ~600-nm-thick overcoat to minimize friction and wear. Among the widely used overcoats, namely, silicon nitride (SiN_x), chromium oxide (CrO_x), chromium nitride (CrN_x), amorphous carbon (a-C), zirconium oxides (ZrO_2 and Zr_2O_3), and their various combinations, most of them suffer from excessive wear and friction despite being quite thick (*10*–*19*). Wear and friction issues are particularly critical for TDs owing to their contact recording architecture, where the recording head is always kept in contact with the tape media that slides across the head (*9*, *12*–*17*). As a consequence, the tape head experiences severe wear and, over time, induces a large pole tip recession, leading to an increased magnetic spacing, degradation of recording functionality, and, subsequently, early failure of the TD (*12*–*17*). Most ~20- to 100-nm-thick coatings showed poor wear resistance and/or survived less than ~1.7 to 5 million meters (Mm) of tape sliding in tape head wear (THW) tests, with a-C films grown by energetic processes demonstrating relatively better wear resistance (*12*–*19*). Hence, improving the wear resistance of overcoats at reduced thicknesses is one of the most fundamental requirements to increase the storage capacities and operational lifetime of TDs (*9*, *17*).

In general, the development of a single sub–10-nm-thick overcoat to largely modify friction and wear in the nano-, micro-, and macroscales is of huge interest for many current and future applications such as TDs, MEMS/NEMS, AFM tips, and other common tribological applications. However, doing so continues to be challenging as the structural, tribological, and protective characteristics of these overcoats diminish notably at sub-10-nm thicknesses (*4*, *8*, *12*, *18*–*24*). Here, we propose a novel method of atomic intermixing and precise tailoring of the nanoscale interfaces in ~7- to 8-nm-thick C/SiN_x multilayer overcoats via depositing C and SiN_x layers alternately and using a high-energy carbon treatment to largely control wear and friction at all tribological length scales. By extensive optimization, we develop a new type of overcoat comprising

[1]Department of Electrical and Computer Engineering, National University of Singapore, Singapore 117583, Republic of Singapore. [2]Institute of Materials, Ecole Polytechnique Fédérale de Lausanne (EPFL), 1015 Lausanne, Switzerland. [3]Singapore Eye Research Institute, Singapore 169856, Republic of Singapore. [4]Hysitron Inc., 10025 Valley Road, Minneapolis, MN 55344, USA. [5]Institute of Materials Research and Engineering, A*STAR (Agency for Science, Technology, and Research), 2 Fusionopolis Way, Innovis #08-03, Singapore 138634, Republic of Singapore. [6]Western Digital Company, Recording Sub System Staging and Research, San Jose, CA 95135, USA. [7]Center for Nanoscale Materials, Argonne National Laboratory, 9700 S Cass Avenue, Argonne, IL 60439, USA.
*Corresponding author. Email: neerajdwivedi6@gmail.com (N.D.); elebcs@nus.edu.sg (C.S.B.)

two consecutive cycles of 0.7-nm SiN_x/high-energy carbon treatment/2.75-nm carbon (90 eV) (sample M, Fig. 1A), yielding super-high wear resistance and low-friction characteristics at the nano- and microscale on a flat Al_2O_3 + TiC (AlTiC) composite ceramic substrate, as well as high macroscale wear durability on a tape head, despite being only ~7 to 8 nm in thickness.

RESULTS AND DISCUSSION

Atomic intermixing and tailoring of nanoscale interfaces

Since carbon has strong affinity with both silicon and nitrogen, we hypothesized that the creation of robust interfaces, atomic intermixing, and tailoring of nanoscale interfaces can be performed by the deposition of ultrathin SiN_x and carbon layers alternately while varying their thicknesses and tuning the energetics of the arriving carbon atoms/ions. We executed our experiments in view of this proposed concept and deposited alternating SiN_x layers (thicknesses of ~0.7 to 1.5 nm) and carbon layers (thicknesses of ~2 to 2.75 nm at 4 and 90 eV) for 2 cycles, without and with high-energy carbon treatment (T_n) at 350 eV (Fig. 1A) (see Supplementary Discussions 1 and 2). Here, 4 eV is the energy of sputter-processed carbon, while 90 and 350 eV are the energies of carbon processed by a filtered cathodic vacuum arc (FCVA) (*4*, *25*). The thickness of the overcoat is a critical parameter to us because the development of many technologies is directly linked to the reduction of the overcoat thickness. The intended thickness of these overcoats is kept to ~7 to 8 nm, which is in the ultrathin regime. Hence, even a modest alteration of overcoat thickness in this regime can cause a big change in the percentage scale, unlike overcoats with hundreds of nanometers in thickness. Therefore, we used high-resolution transmission electron microscopy (HRTEM) to directly and accurately measure the thickness of these overcoats grown on Si substrates. Fig. 1B shows the HRTEM images of a few selected samples (see Supplementary Discussion 3 for additional details and HRTEM images of all samples). We applied capping layers of tantalum before and after the overcoats are deposited on the Si substrates specifically for the HRTEM cross-sectional imaging measurements. This was done because the lighter contrasts of both carbon and SiN_x are similar to the native

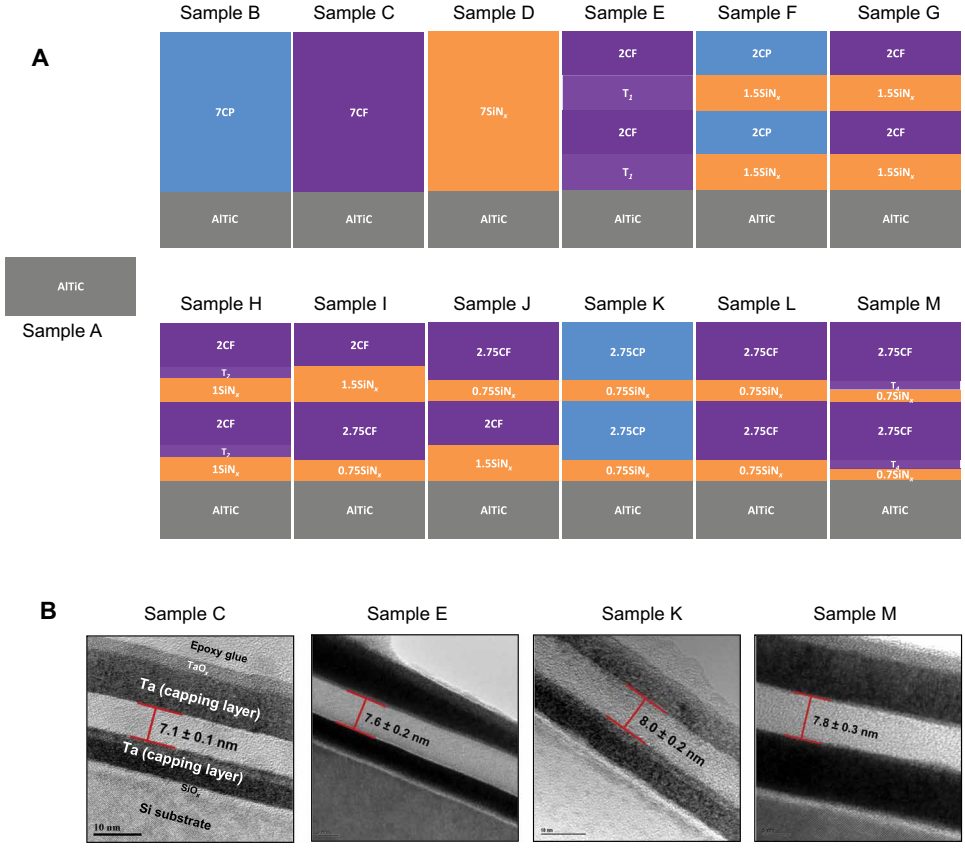

Fig. 1. Schematics of test samples and HRTEM images. (**A**) Schematics of the overcoat designs: Monolithic overcoats 7CP (sample B), 7CF (sample C), and 7SiN_x (sample D); carbon superlattice overcoat 2(T_1/2CF) (sample E); C/SiN_x multilayer overcoats 2(1.5SiN_x/2CP) (sample F), 2(1.5SiN_x/2CF) (sample G), 2(1SiN_x/T_2/2CF) (sample H), 0.75SiN_x/2.75CF/1.5SiN_x/2CF (sample I), 1.5SiN_x/2CF/0.75SiN_x/2.75CF (sample J), 2(0.75SiN_x/2.75CP) (sample K), 2(0.75SiN_x/2.75CF) (sample L), and 2(0.7SiN_x/T_4/2.75CF) (sample M). Sample A is plasma-cleaned bare AlTiC substrate. The prefixed numbers represent the thickness of the respective layer in nanometers, while the letters F and P represent carbon deposition by FCVA (F) and pulsed dc sputtering (P), respectively. High-energy carbon treatment of 350-eV C^+ ions (labeled as T_n, where n = 1, 2, 3, and 4) is performed either to enhance the atomic mixing in the C/SiN_x multilayer overcoats (T_2, T_3, and T_4) or to construct a carbon superlattice structure (T_1, where T_1 adds 1.5 nm carbon thickness). The deposition times for T_2, T_3, and T_4 are adjusted in such a way that they contribute to <1-, <0.3-, and <0.5-nm thicknesses, respectively, to the total overcoat thickness. (**B**) Cross-sectional HRTEM images with measurements of the overcoat thickness in samples C, E, K, and M. In all images, capping layers of tantalum (Ta) are deposited by magnetron sputtering before and after overcoat deposition on Si wafer substrates, as labeled, to provide image contrast for accurate overcoat thickness determination.

SiO_x layer on Si and the epoxy layer used to glue the sample during sample preparation. On the other hand, tantalum as a capping layer shows darker contrast in HRTEM. Thus, the cross-sectional HRTEM samples with the tantalum capping layers assist in accurately determining the thickness of the overcoat by eliminating the regions of epoxy and SiO_x. Therefore, in all the samples, the overcoat thickness can be measured between the two capping layers (Fig. 1B). The total thicknesses of these composite nanoscale multilayer structures were measured to be ~7 to 8 nm, which were in agreement with the expected thicknesses.

The general picture of atomic mixing and the creation and tailoring of nanoscale interfaces were first visualized theoretically by performing Monte Carlo–based transport and range of ions in matter (TRIM) calculations (*26*). We observed that the volume of interaction significantly increases with increasing the energy of the carbon ions/atoms arriving at the substrate and with the reduction of the SiN_x layer thickness, resulting in an enhanced distribution of carbon in the interlayer and substrate regions as well as increased recoiling of the interlayer and substrate atoms (see fig. S2A). Next, we simulated the atomic distributions for the actual experimental overcoat designs (Fig. 2, panels 1 to 4). The 4-eV carbon in samples F and K induced a minimal volume of interaction that was limited to the surface of the SiN_x layers. No recoiled atoms from any layer or substrate were observed. In contrast, the application of 90-eV carbon in samples G, I, J, and L led to a much higher volume of interaction with the observation of recoiled atoms from the intermediate layers and the substrate. However, when 350-eV carbon ions were introduced for a short span of time (see Fig. 1 caption) in combination with 90-eV carbon ions in samples H, M, and E, the volume of interaction and number of recoiled atoms were markedly increased (see Supplementary Discussion 4 for the comprehensive TRIM calculations). Thus, FCVA-processed carbon allows extensive atomic intermixing and the creation of relatively more mixed interfaces than its sputtered counterpart.

Next, we used x-ray photoelectron spectroscopy (XPS) (Fig. 3) and Auger electron spectroscopy (AES) depth profiles (graphs shown in section "Engineering and controlling the wear on commercial TD heads") to qualitatively probe the intrinsic structure and composition of the overcoats and, in doing so, gain an insight into the interface tailoring and atomic mixing. The AES depth profiles revealed the presence of C, Si, and N in the overcoat region as evident from their higher intensities up to the overcoat/substrate interface region. Beyond the overcoat/substrate interface region toward greater sputter times (depths), the intensities of O, Al, and Ti started to increase and eventually reached a saturated level, which is in agreement with the expected composition of the AlTiC substrate. In the overcoat region, the variation of the elemental compositions of C, Si, and N with sputter time (or depth) appeared to be consistent with the expected layered composition of the overcoat. The AES depth profiles show that there is one interface (I) at the film/substrate boundary for monolithic overcoats (samples B and C) and four interfaces at each boundary for all C/SiN_x multilayer structures, i.e., $C/I_1/SiN_x/I_2/C/I_3/SiN_x/I_4$/substrate, which are in agreement with the prepared C/SiN_x multilayer designs. Each interface region was observed to be highly mixed (i.e., interfaces are not abrupt) as a result of atomic intermixing.

Furthermore, we recorded various high-resolution XPS spectra at different depth levels and thoroughly examined all the XPS results (see Supplementary Discussions 5 and 6). We present the results of the deconvoluted high-resolution XPS spectra of C 1s, Si 2p, N 1s, Ti 2p, and Al 2p for C/SiN_x multilayer samples G, L, and M (Fig. 3, A to F). From figs. S3 (before deconvolution) and S4 (A to I) (after deconvolution), we noticed that the signals related to the substrate atoms (Al 2p and Ti 2p peaks, as well as the Ti-C peak in the C 1s spectra) were negligible when the XPS spectra were recorded without performing a depth profile (0 s), because of the limited photoelectron escape depth. Therefore, high-resolution spectra were recorded at different depth levels to examine the chemical bonds present at the film/substrate (FS) interface. A comprehensive analysis of chemical and interfacial bonding as a function of different etching times for samples G, L, and M (fig. S4, A to I), together with chemical bonding analyses of additional samples H and K (fig. S4J), can be found in Supplementary Discussion 6. Since the XPS photoelectron escape depth was large enough to examine the top C/SiN_x layers (mainly the top two to three layers), the chemical bonds based on C/Si/N atoms can be visualized even without depth profiling. On the basis of the signal for Ti–C bonding (arising from the AlTiC substrate) in the C 1s spectra, the etching times required to reach the FS interfaces and substrate regions were determined, which varied from sample to sample (i.e., 100 s for sample G, 125 s for sample L, and 150 s for sample M). Here, in Fig. 3 (A to F), we present the deconvoluted XPS spectra of samples G, L, and M that were measured as-received before etching (0 s), as well as after their respective etching times to reach the FS interface. Except Ti-C peak, the C 1s spectra recorded without performing a depth profile (0 s) showed Si–C, sp^2C, sp^3C, C–O, and C═O bonding peaks for all the C/SiN_x multilayer samples. However, the C 1s spectra recorded after etching time of 100 s for sample G, 125 s for sample L, and 150 s for sample M showed Ti–C peak, in addition to other peaks, as the substrate is approached. Other types of bonding are evident from the Si 2p, N 1s, Ti 2p, and Al 2p spectra. The Al–O and Ti–C peaks correspond to the AlTiC substrate, whereas Si–N is assigned to the SiN_x layers. Various carbon–carbon and carbon–oxygen bonds reveal the tuning of carbon chemistry and carbon hybridization. New hybrid interfacial bonds, namely, Si–C, Si–O/Si–O–N, (Al, Ti)N, sp^3C–N/Nitrile/Si–O–N, sp^2C–N, (Ti, Al)N/Ti–C–O–Al–N, (Ti, Al)N–O, and Al–N were created. Thus, apart from the intrinsic bonds present in the layer/substrate material, we achieved the creation of several new hybrid interfacial bonds as a consequence of interfacial chemical interactions between different layers, as well as between the layer(s) and the substrate. FCVA-processed C/SiN_x multilayer structures yielded more interfacial bonding than sputter-processed C/SiN_x multilayer structures due to the use of higher carbon energies, which corroborates with the TRIM calculations. As an example, to compare the interfacial bonding between FCVA-processed and sputter-based C/SiN_x multilayer overcoats with similar carbon thickness (2.75 nm in each layer) and SiN_x thickness (0.75 nm in each layer), we estimated the amount of interfacial Si–C bonding from the Si 2p spectra for sample K (sputtered C/SiN_x multilayer overcoat) and sample L (FCVA-processed C/SiN_x multilayer overcoat). The bonding fraction of Si–C bonds was estimated to be 18.6% in sample K, which was markedly increased to 45.5% in sample L, confirming that the FCVA-processed C/SiN_x multilayer overcoats tend to form a greater amount of interfacial bonds.

Since sp^3 bonding is an important structural parameter that influences the functional properties of amorphous carbon films (*24*, *25*, *27*–*30*), we measured sp^3 bonding using Raman spectroscopy based on the movement of the G peak under ultraviolet excitation

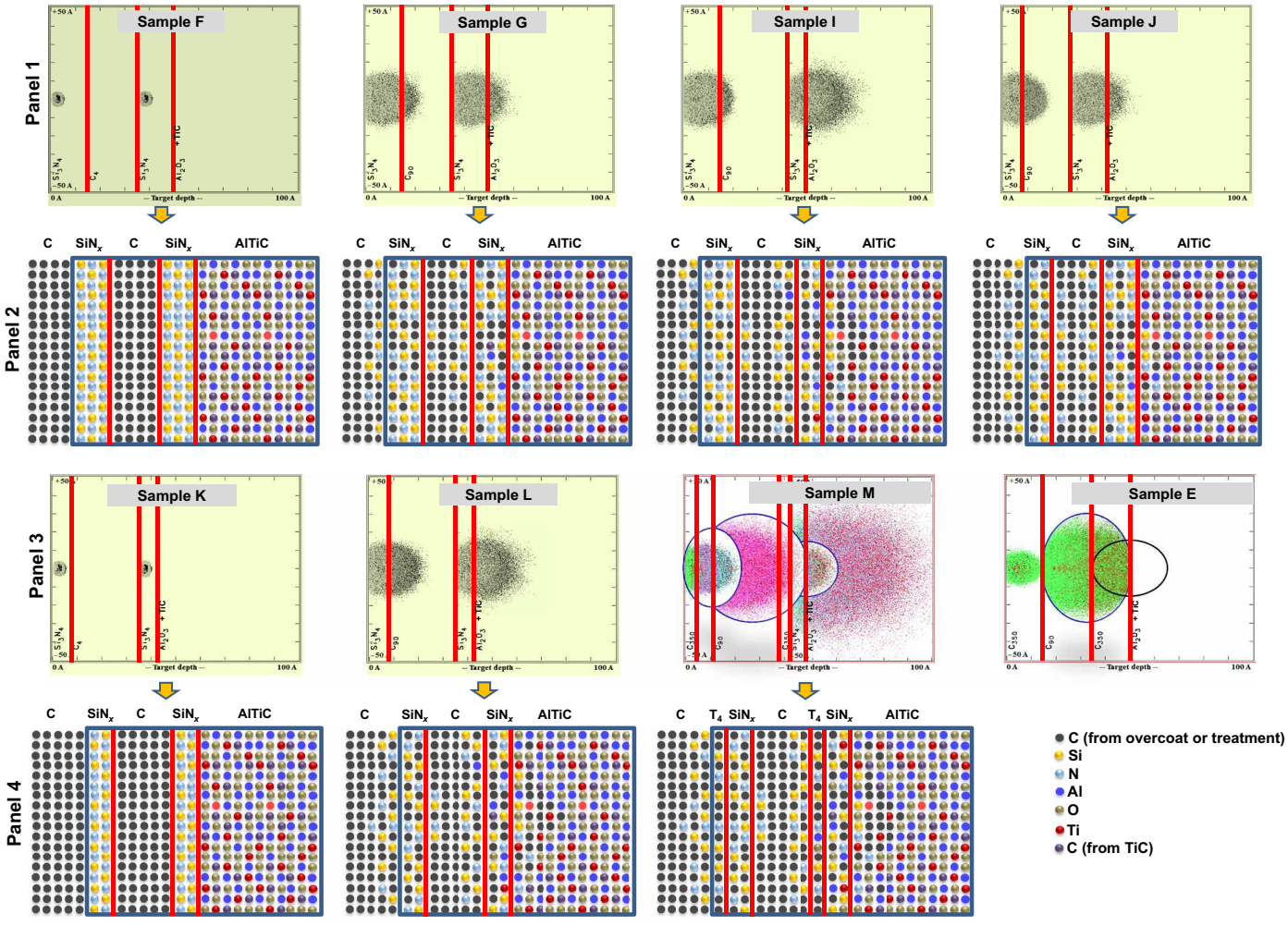

Fig. 2. TRIM simulations. TRIM simulations for selected samples showing the extent of atomic mixing and recoils in the depth profile plots, illustrated using color-coded schematics below each plot (panels 1 to 4). Stoichiometric Si_3N_4 is available in the TRIM directory and was used to mimic the experimentally grown SiN_x. The thickness of SiN_x was varied from 1.5 to 0.7 nm, and the energy of incoming carbon atoms was changed from 4 to 350 eV during the TRIM calculations to simulate the experimental structures.

following the three-stage model (*25*, *28*) and also by deconvolution of the high-resolution XPS C 1s spectra (*28*, *31*) (Fig. 3G; see Supplementary Discussion 7 for a detailed discussion). Spectroscopic analyses showed that FCVA-processed monolithic carbon and C/SiN_x multilayer structures have carbon microstructures containing much higher sp^3 carbon bonding and less ring-like sp^2 carbon networks than their sputtered counterparts. For example, when comparing C/SiN_x multilayer samples K and L, while both samples have similar carbon thickness (2.75 nm in each layer) and SiN_x thickness (0.75 nm in each layer) stack, the sp^3 bonding is about three times higher (~59%) in sample L than in sample K (~21.5%). This is because the energetics of carbon in FCVA (90 eV) facilitate subsurface growth and hence subplantation (*28*, *31*), resulting in higher sp^3 bonding than sputtered carbon (<5 eV). Among the FCVA-processed C/SiN_x multilayer overcoats, the sp^3 bonding was observed to increase with increasing 90-eV carbon layer thickness from 2 nm per carbon layer (samples G and H) to 2.75 nm per carbon layer (samples L and M). Ball-and-stick chemical models (Fig. 3H) were also prepared on the basis of the Raman results, showing higher sp^3 bonding and negligible ring-like sp^2 carbon network for FCVA-processed carbons (samples C and E) and vice versa for sputter-deposited carbon (sample B). Thus, the increased overcoat robustness due to increased interfacial strength between the layers in the overcoat, enhanced FS robustness, improved adhesion of overcoat with substrate, and tuning of the carbon microstructure (high sp^3 versus low sp^3) are expected to have a substantial influence on the overcoat's resistance to contact sliding at the nano-, micro-, and macroscales.

Nanoscale surface, mechanical, and tribological properties

The root-mean-square surface roughness (R_q) of bare and coated AlTiC, measured using AFM, is shown in Fig. 4A. The R_q of uncoated AlTiC was measured to be ~8 nm. In comparison, the overcoated AlTiC samples also showed an R_q of ~6 to 8 nm. Since amorphous carbon is an intrinsically smooth material (*20*, *21*), the origin of the large R_q for these coated samples is mainly due to the pronounced influence of the AlTiC substrate roughness. This is evident when comparing the roughness of auxiliary C/SiN_x bilayer overcoats deposited on both rougher AlTiC and smoother Si wafer substrates, whereby a much lower R_q (~0.1 to 0.2 nm) was obtained for the overcoats on Si (see Supplementary Discussion 8). Thus, the carbon-based overcoats are intrinsically smooth. The roughness profiles of uncoated AlTiC and AlTiC coated with a few selected overcoats are presented in Supplementary Discussion 8.

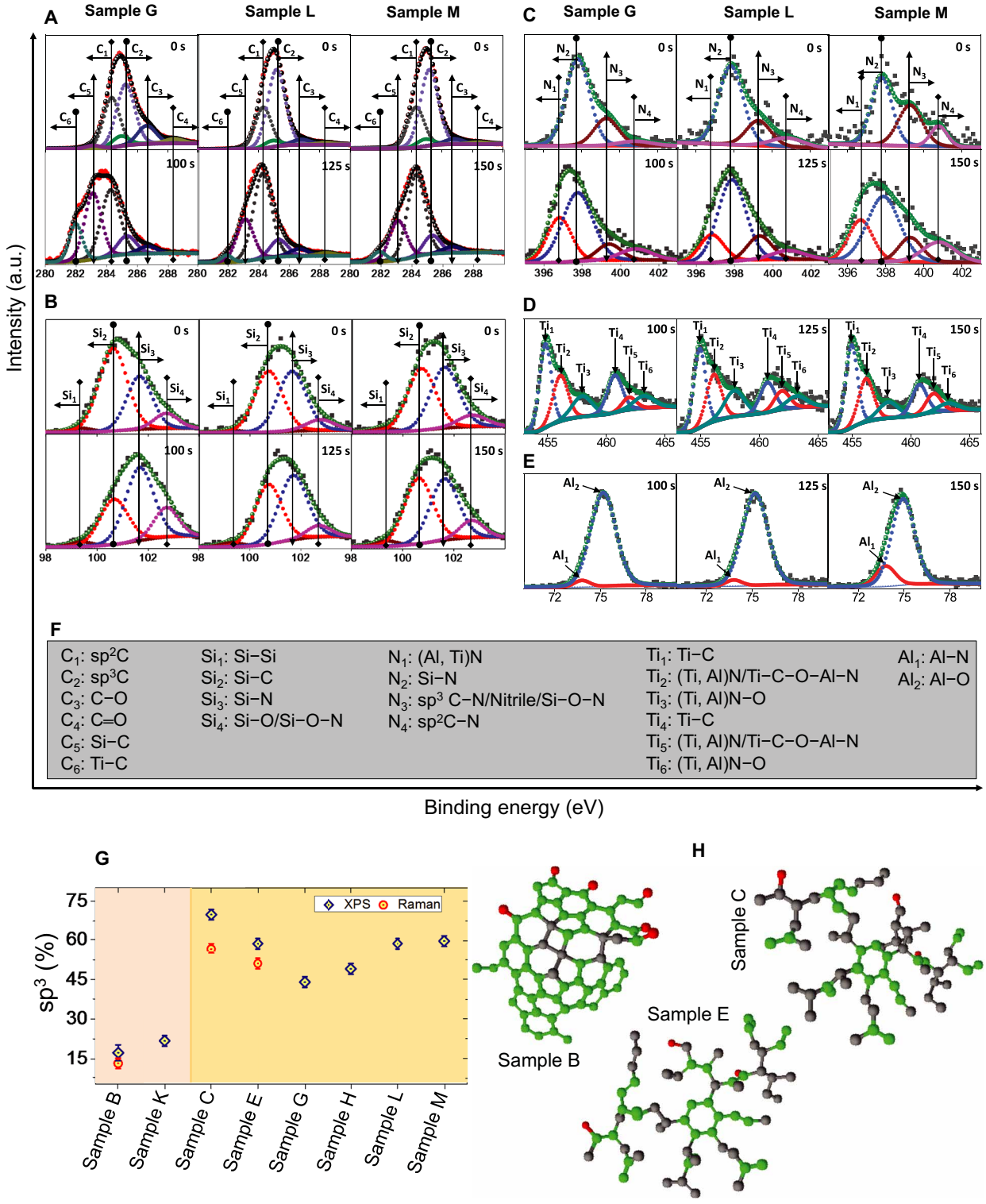

Fig. 3. Interfacial and structural properties. Deconvolution of various XPS core level spectra recorded without performing a depth profile (0 s) and after an etching time of 100 s for sample G, 125 s for sample L, and 150 s for sample M. (**A**) Deconvolution of C 1s spectra for sample G (0 and 100 s), sample L (0 and 125 s), and sample M (0 and 150 s). (**B**) Deconvolution of Si 2p spectra for sample G (0 and 100 s), sample L (0 and 125 s), and sample M (0 and 150 s). (**C**) Deconvolution of N 1s spectra for sample G (0 and 100 s), sample L (0 and 125 s), and sample M (0 and 150 s). (**D**) Deconvolution of Ti 2p spectra for sample G (100 s), sample L (125 s), and sample M (150 s). (**E**) Deconvolution of Al 2p spectra for sample G (100 s), sample L (125 s), and sample M (150 s). (**F**) Different peaks corresponding to the different chemical bonding species. (**G**) Variation of sp^3C bonding based on Raman and XPS analyses. The three-stage model, proposed by Ferrari and Robertson (*25*), was used to estimate sp^3 bonding by Raman spectroscopy. (**H**) Ball-and-stick chemical models for samples B, C, and E. Lime, gray, and red color balls correspond to sp^2-carbon, sp^3-carbon, and oxygen atoms, respectively.

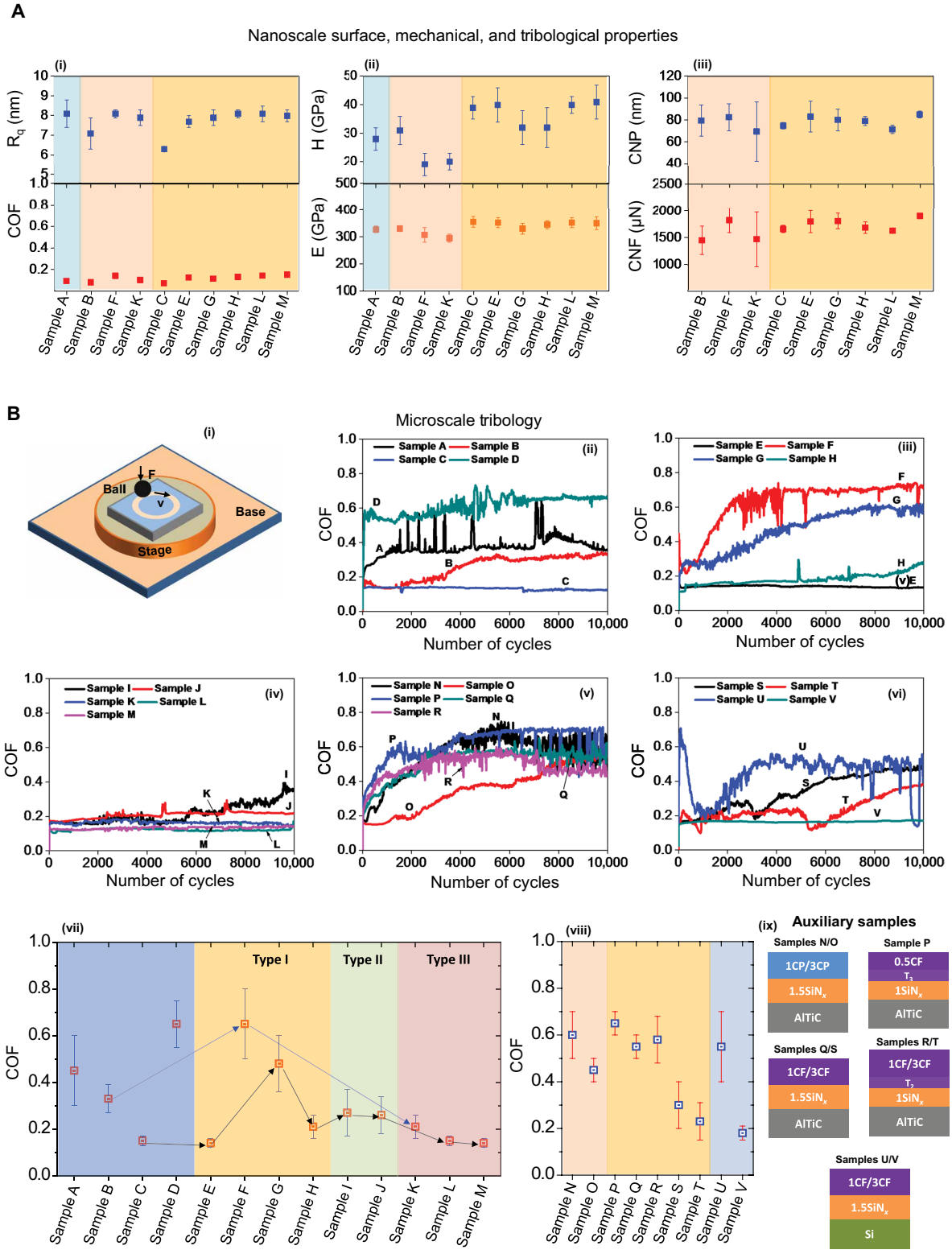

Fig. 4. Surface, mechanical, and tribological properties. (**A**) (i) R_q and nanoscale friction, (ii) hardness and elastic modulus, and (iii) CNP and CNF for various samples. (**B**) (i) Schematic of the experimental setup for ball-on-disk tribological tests. (ii to ix) Ball-on-disk microscale tribology showing the frictional curves and COF values for different samples. One cycle corresponds to a distance of 1.257 cm. All the experimental conditions were kept the same to limit any external influence on microscale tribology (see Materials and Methods and Supplementary Discussion 2). The nanoscale COF was found to be similar in these samples, although closer inspection revealed that it was marginally higher in the carbon superlattice overcoat (sample E) and C/SiN_x multilayer overcoats than in the monolithic carbon overcoats (samples B and C). Furthermore, in a microscale friction test environment, sample M exhibited the lowest and most stable friction.

Next, we examined the nanomechanical properties [hardness (H) and elastic modulus (E)] and nanotribological properties [nanoscale coefficient of friction (COF) and nanoscratch resistance] of these samples (Fig. 4A). AFM topography images were recorded from various locations before and after nanoindentation and nanoscratch tests to visualize the indent/scratch marks (see Supplementary Discussion 9). Although the measured mechanical properties show a significant substrate influence due to the extremely low thickness of the overcoats, we observed that the H and E values were higher for the FCVA-processed carbon-based samples than that for the sputter-coated counterparts due to the presence of higher sp^3 carbon bonding in the former. Furthermore, all these samples, including bare AlTiC, showed very low and similar nanoscale friction (COF < 0.2), indicating that carbon microstructure and interface chemistry do not have much influence on the nanoscale friction. To assess the nanoscale scratch resistance, we measured the average critical normal force (CNF) and critical normal displacement (CNP) (*9*). The CNP and CNF are measured at the onset of critical events, with higher values corresponding to a better scratch resistance (*9*). Carbon superlattice sample E and the C/SiN_x multilayer samples with higher SiN_x thickness revealed better nanoscratch resistance than the monolithic carbon overcoats. The reduction of SiN_x thickness decreased the nanoscratch resistance (as seen in samples K and L), but the application of high-energy carbon treatment in conjunction with lower (higher) SiN_x (carbon) thickness gave the highest nanoscratch resistance (sample M). We demonstrate a crucial finding here that the increased interfacial strength/adhesion is the key parameter for obtaining excellent nanoscratch resistance, followed by the availability of higher sp^3 carbon bonding.

Controlling and engineering microscale wear and friction

We performed microscale ball-on-disk tribological measurements to understand how the creation of multiple interfaces and associated atomic intermixing and tailoring of nanoscale interfaces control the friction and wear of carbon-based overcoats (Figs. 4B and 5A). The friction of the sample is judged on the basis of the COF and stability of the frictional curves where a lower value of COF and higher stability (or less fluctuations) of the frictional curves signify a better overcoat. A better wear resistance correlates with a faint wear track on sample surface and less debris transfer to the ball. Bare AlTiC gave a fluctuating frictional curve with a high COF (>0.4), which was reduced by ~27 and ~67% after the application of monolithic carbon in samples B and C, respectively. Bare AlTiC also showed significant wear that was reduced in sample B and was barely visible in sample C. This suggested that overcoats are necessarily required to mitigate friction and wear. In contrast, monolithic SiN_x showed the highest COF (~0.65) with continuous fluctuations throughout the measurement and resulted in extremely high wear. Overall, monolithic carbon deposited at moderate energy (90 eV) by FCVA demonstrated the lowest wear and friction of all the monolithic overcoats.

Next, we classified the carbon superlattice and C/SiN_x multilayer samples into three types to present and explain their microscale tribological behavior. In type I, samples E, F, G, and H are included, which contain ~2-nm-thick carbon layers in the lower and upper sides of the multilayer/superlattice stacks. Carbon superlattice sample E showed very low COF (~0.14) and a stable frictional curve with high wear resistance. In contrast, the C/SiN_x multilayer structures in designs F and G demonstrated significantly higher and fluctuating friction with very severe wear, which is totally opposite to what was observed with their nanoscale friction and nanoscratch tests, thus displaying two mutually conflicting behaviors (see Figs. 4, A and B, and 5A). However, when the C/SiN_x multilayer overcoat design was slightly tailored in sample H, it yielded significantly reduced microscale friction and wear. This prompted us to prepare and test several auxiliary C/SiN_x bilayer overcoats (Fig. 4B,v, vi, viii, and ix) with varied layer thicknesses of SiN_x and carbon, and with varied T_n, to produce more effective overcoat designs. The results for the auxiliary C/SiN_x bilayer samples suggest that, for effective tribological coatings, the carbon thickness should be close to 3 nm, SiN_x thickness needs to be low, and high-energy carbon treatment should be performed (see Supplementary Discussion 10 for details).

Taking the knowledge obtained from the tribological analysis of auxiliary samples, we move to type II samples I and J, which have thicker carbon (~2.75 nm) and thinner SiN_x (~0.75 nm) on either the lower or the upper side of the C/SiN_x multilayer stacks. The tribological results are consistent with the conclusions drawn from the auxiliary sample analysis, as samples I and J demonstrated significantly lower friction and wear than sample G, with sample J slightly outperforming sample I. These results inspired the design of type III samples, which include samples K, L, and M that have 0.7- to 0.75-nm-thick SiN_x and 2.75-nm-thick carbon layers for both of the lower and upper sides of the multilayer stacks. These type III samples eventually showed further reduction of friction and wear. Sample K yielded ~68 and ~36% lower friction than samples F and B, respectively. Similarly, sample L yielded ~69% lower friction than sample G. Among all overcoats, type III sample M yielded the best microscale tribological performance in terms of very low and stable friction (COF, ~0.14) and super-high wear resistance. Earlier, it was noted that sample M also outperformed all samples in nanoscale friction and nanoscratch test environments. This shows that a multilayer stack with thinner SiN_x (~0.7 nm) and thicker carbon (~2.75 nm) deposited at a carbon ion energy of 90 eV with a high-energy (350 eV) carbon treatment, such as T_4, is pivotal for obtaining extraordinary friction and wear properties on both the micro- and nanoscale.

We repeated the microscale tribological tests many times for the reproducibility of the results (see Supplementary Discussion 10) and examined the wear tracks by Raman spectroscopy to uncover the underlying mechanisms. We present the wear track analyses of a few selected samples by Raman spectroscopy in Fig. 5B. Among the sputter-processed C/SiN_x multilayer overcoats, sample K showed relatively less structural damage and wear of carbon than sample F, as defined by comparing the shapes of the spectra outside and on the wear track. Similarly, among the FCVA-processed C/SiN_x multilayer overcoats, sample J showed relatively less structural damage and wear of carbon than sample G. In general, the Raman results showed significant damage and removal of carbon for the overcoats whose wear tracks were found to be most severe in the optical microscope images (see Supplementary Discussion 11 for detailed Raman analysis). In addition, some degree of wear-induced $sp^3 \rightarrow sp^2$ bonding transformation was also observed in these overcoats.

Engineering and controlling the wear on commercial TD heads

These ~7- to 8-nm-thick overcoats were applied onto TD heads to test their wear resistance in a rigorous macroscale THW test environment. The THW tests closely mimic the operation of actual TDs where overcoated heads are exposed to magnetic tape sliding for a long period of time (*12*) (Fig. 6A; see Supplementary Discussion 12).

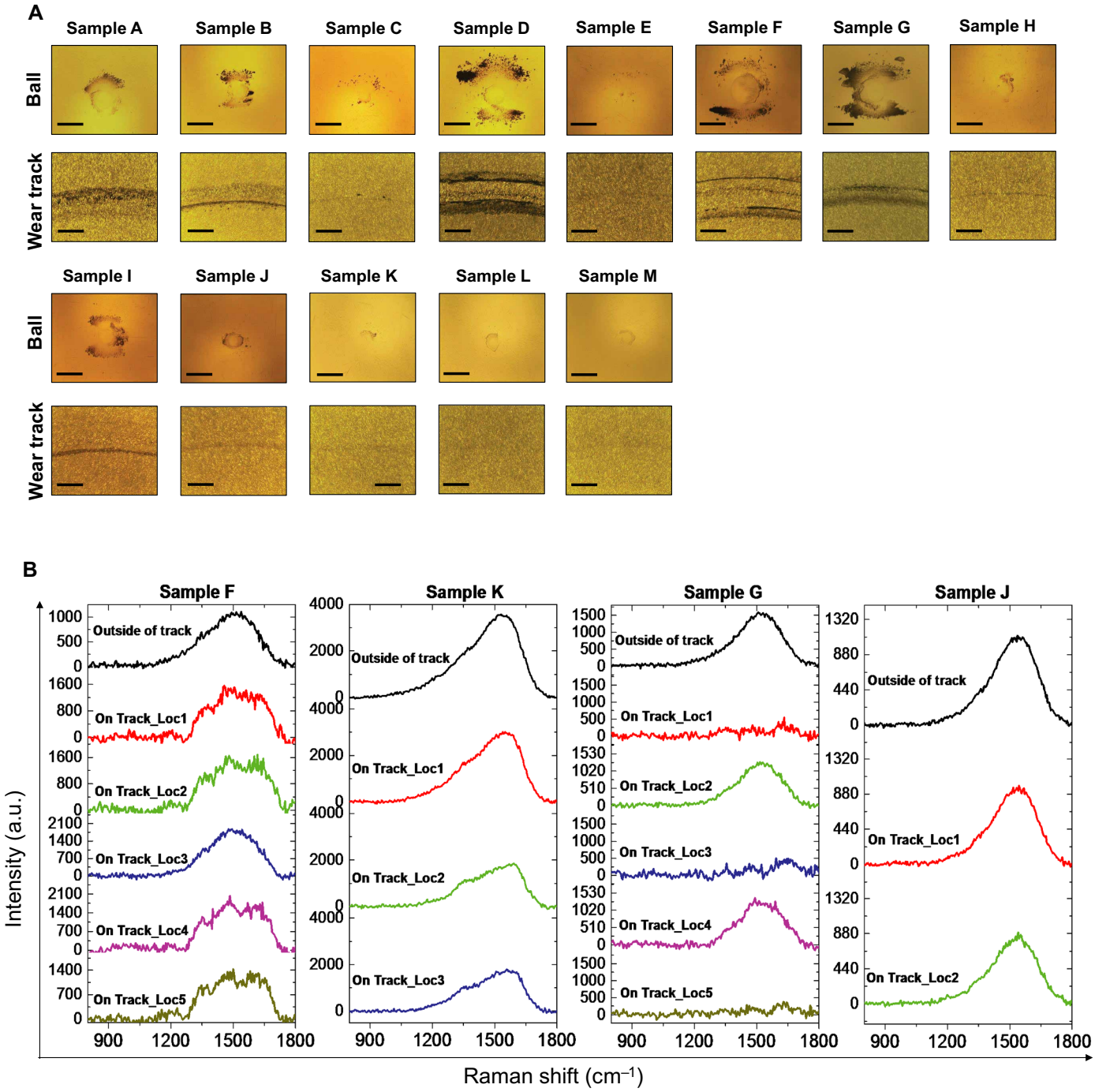

Fig. 5. Wear analysis after microscale ball-on-disk tribological tests. (**A**) Optical images of the balls (rows 1 and 3) and sample surfaces (rows 2 and 4) after the tribological measurements. The images reveal the amount of debris transferred to the balls and the severity of the wear tracks formed on the sample surfaces. Scale bars, 100 μm. Bare AlTiC showed significant wear, whereas sample M yielded the least wear. (**B**) Raman spectra of selected samples recorded from outside the wear track and at various locations (Loc) on the wear track to examine the wear in relation to the overcoat design. The sputter-processed C/SiN_x multilayer in sample F experienced significant wear, indicating a considerable amount of overcoat removal and damage to the carbon layers, as visualized by the noisy Raman spectra on the wear tracks when compared to outside of the wear track. However, the wear was minimized in sample K because of the tailoring of the carbon and SiN_x thicknesses, resulting in a small amount of carbon removal and minor structural damage to the carbon layers, although a D peak emerged when Raman spectra were recorded from the wear tracks, suggesting a higher amount of disordered sp^2 carbon. A similar behavior to the sputter-processed overcoats was observed for the FCVA-processed C/SiN_x multilayers, where sample G showed higher wear, but the wear was minimized by tuning the carbon and SiN_x thicknesses in sample J (see Supplementary Discussion 11 for a detailed wear track analysis by Raman spectroscopy).

These tests were performed up to a tape sliding distance of 5 Mm. After 5 Mm of THW testing, most of the overcoats were completely worn off except samples C, E, and M (see Supplementary Discussion 12 for detailed analyses). Optical microscope images of the heads with the three best-performing overcoats before the THW test (0 Mm) and after test durations of 1, 2, and 5 Mm of THW from the same location of each sample are shown in Fig. 6B. The images reveal the tape head architecture: the AlTiC substrate and closure, an Al_2O_3 dielectric gap (middle dark gray strip extending in the horizontal direction), and the magnetic read/write poles and shields in the Al_2O_3 gap region. We observed, in general, that as the tape test progressed, the overcoat experienced increasing wear with THW test duration. Monolithic FCVA-processed carbon (sample C) experienced significant wear near the AlTiC substrate/closure edges, as shown by discoloration in the optical images and pointed out in Fig. 6B. On the contrary, the C/SiN_x multilayer overcoat in sample M and carbon superlattice sample E demonstrated extraordinary wear resistance, as most of the coating in each case was still present on the entire area of the head after the THW test.

We used AES imaging and AES depth profiling to obtain a greater insight into the wear durabilities of the overcoated heads. We present here the AES images (Fig. 6C) and AES depth profiles (Fig. 7) for four selected samples C, E, G, and M, while the complete AES analysis with AES images and depth profiles of eight samples (namely, samples C, E, F, G, H, K, L, and M) can be found in Supplementary Discussion 12. In the AES images, the elements C, O, Al, and Si were mapped. AES images revealed that, apart from samples C, E, and M, all the other overcoats were completely removed

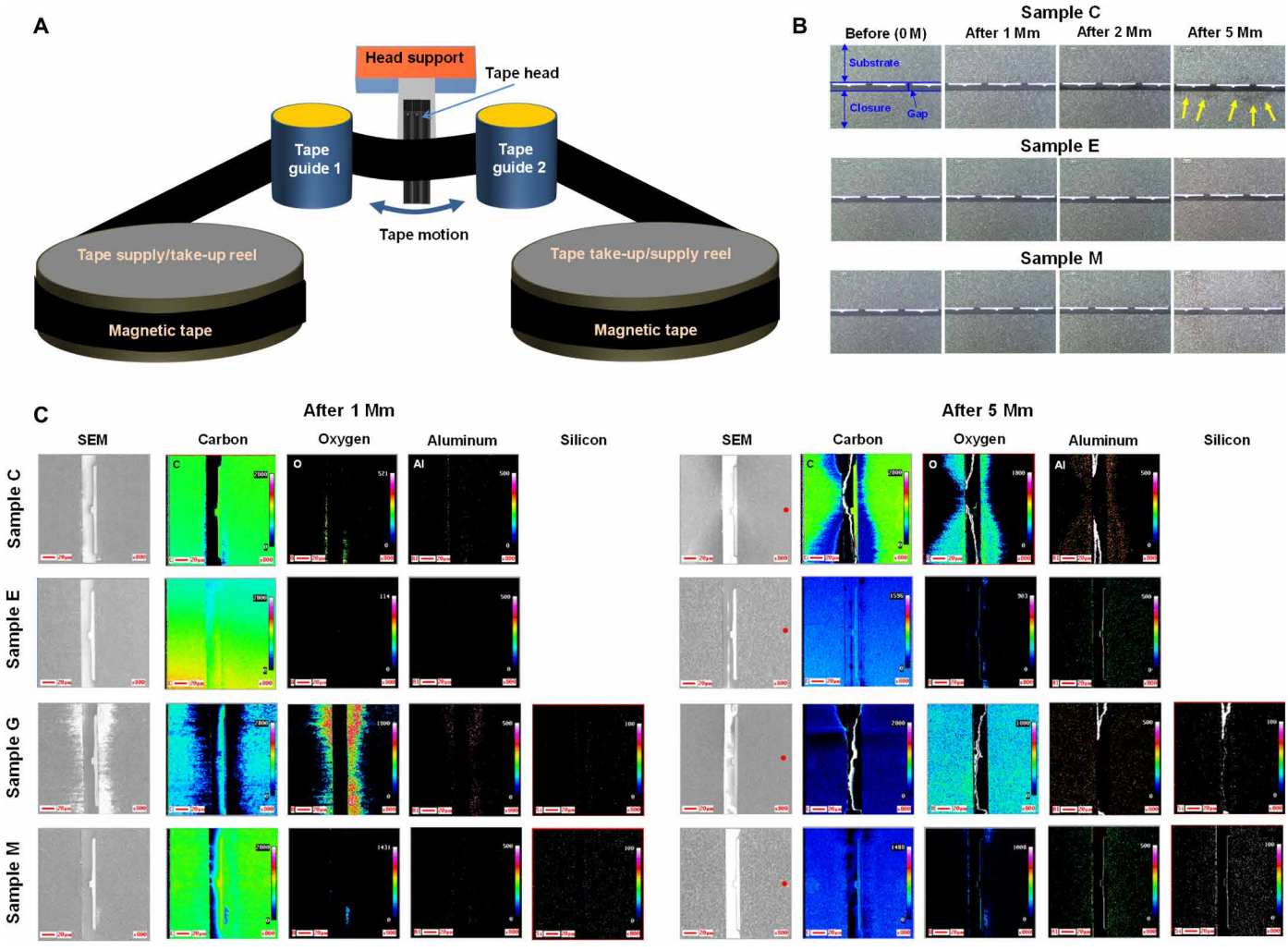

Fig. 6. Long-term THW test and wear analysis. (**A**) Schematic of the THW test setup used in the present work comprising tape supply/take-up reel components, tape guides, and the tape head to be tested, which was kept in contact with the sliding tape media at a constant tension. This simulates the operation of actual TDs. Since most of the previous thicker (~20 to 100 nm) overcoats could survive up to a maximum of 1.7 to 5 Mm of tape sliding in the THW test, we performed THW tests up to a tape sliding distance of 5 Mm to analyze the wear of our ~7- to 8-nm overcoats. (**B**) Optical microscope images of selected tape heads after THW tests. The brighter and darker portions indicate the presence and removal of overcoats, respectively. Although sample G demonstrated good wear resistance, it yielded very severe wear near the AlTiC substrate/closure edges adjacent to the Al_2O_3 gap region and inside the gap. In contrast, the wear was found to be minimal in samples E and M, suggesting higher wear resistance. (**C**) AES images to assess wear based on elemental mapping of C, O, Si, and Al. Before AES imaging, SEM images were recorded. The wear was evaluated on the basis of the intensities of C (from the overcoat) and Al/O (from the substrate), where a warmer/brighter color represents higher intensities and cooler/darker color represents lower intensities, according to the color scale bar. The C/SiN_x overcoat in sample M demonstrated the best wear resistance.

after 5 Mm of THW testing, corroborating well with the optical images. Moreover, apart from carbon superlattice sample E and C/SiN_x multilayer sample M, all the other overcoated heads experienced significant amount of charging in the gap region during scanning electron microscopy (SEM) imaging. Only samples E and M had overcoats that were still covering the entire Al_2O_3 gap region and the adjacent AlTiC substrate/closure edges and exhibited uniform wear across the head. While monolithic carbon sample C showed good protection at most locations on the AlTiC, it experienced very nonuniform wear that was most substantial at the AlTiC substrate/closure edges and Al_2O_3 gap region. Since the magnetic read/write poles and shields are contained here, this region is our prime area of interest for wear protection. AES depth profiles (Fig. 7) after 5 Mm of THW tests also confirmed that most of the overcoats had been completely worn off except samples C, E, and M. We calculated that about 65, 48, and 62% of the coating remained on the heads for samples C, E and M, respectively, after the THW tests. Although the amount of coating removed for samples C and M was similar, the locations selected for depth profile analyses were further away from the Al_2O_3 gap and AlTiC substrate/closure edges where sample C showed poorer wear durability. What is interesting here is that sample M showed excellent wear resistance both at the AlTiC substrate/closure edges and Al_2O_3 gap, as well as at the location where the depth profile was performed, which is further away from the area of interest. Thus, on the basis of the wear analyses by optical images, AES maps, and AES depth profiles, we conclude that the C/SiN_x multilayer overcoat design in sample M is the best performing in terms of tape sliding wear durability, followed by the overcoat designs in samples E and C. While studying the wear durability of a 50-nm-thick Cr_2O_3 overcoat, Shi *et al.* (*17*) reported that a significant thickness of the overcoat (7 nm) was removed after just 1 Mm of tape wear. In comparison, our overcoats with just 7 to 8 nm in thickness (samples C, E, and M), and especially sample M, have shown without a doubt to have much higher wear durability than the Cr_2O_3 overcoat. In general, despite being thinner, these three overcoats also fared better in terms of wear durability than thicker overcoats (~20 to 100 nm) (*13*–*19*).

Deterministic parameters and mechanisms for friction and wear

Conventionally, sp^3 bonding is the key parameter that governs wear resistance, while both sp^3/sp^2 bonding and surface chemistry/surface passivation control the friction characteristics of amorphous carbon films (*4*, *6*, *29*–*33*). We uncover here many other novel critical parameters which govern the friction and wear behavior at the sub-10-nm thickness regime on all tribological scales. The interfacial robustness (both within the overcoat and at the overcoat/substrate boundary), increased adhesion, and possession of a critical carbon thickness are found to be the major parameters needed to control and engineer the wear and friction of amorphous carbon–based ultrathin overcoats at all length scales. We also discover that interfacial robustness and critical carbon thickness are mutually interdependent

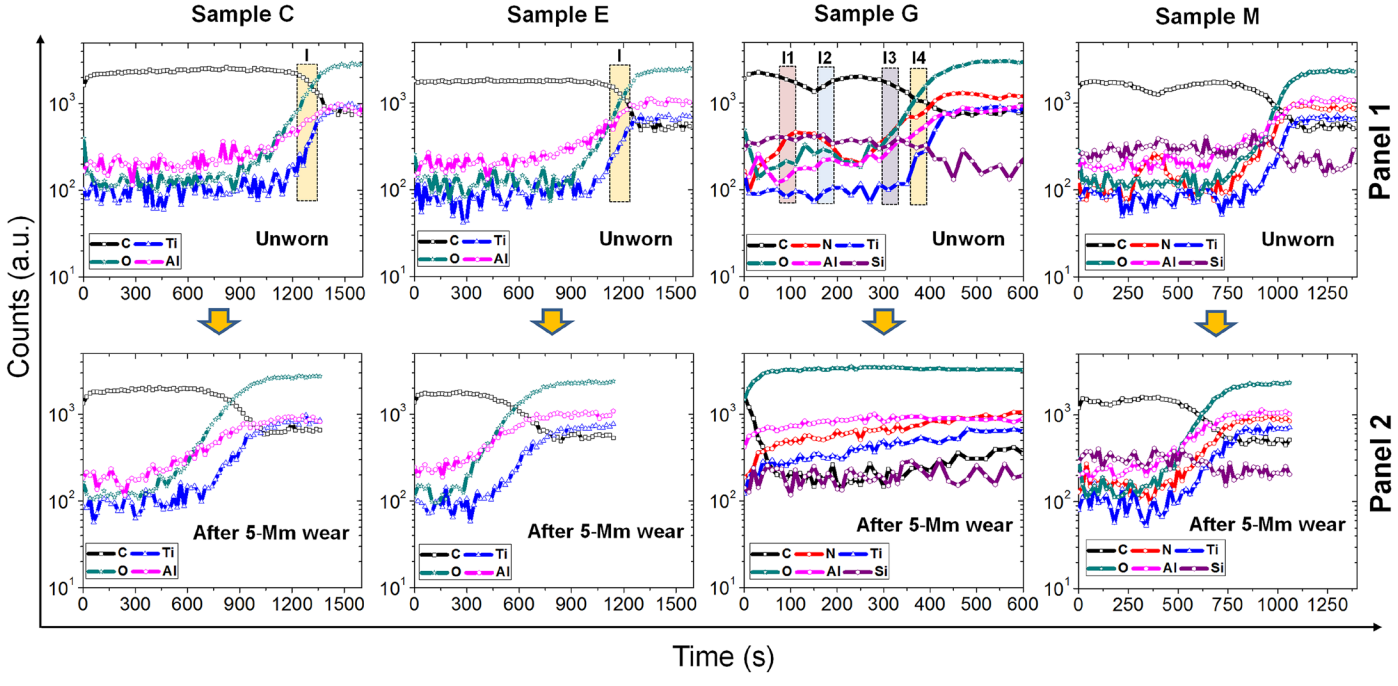

Fig. 7. AES depth profiling to examine overcoat wear after long-term THW tests. After 5 Mm of THW tests, AES depth profiles were performed at selected locations on the head as highlighted by the red dot in each SEM image of Fig. 6C. The corresponding AES depth profile from an unworn region outside of the area of magnetic tape/head interaction for each sample was taken as a reference for comparison purposes. The depth profiles of samples C, E, G, and M are shown here, while those of samples F, H, K, and L are presented in fig. S10D. AES depth profiles for C/SiN_x multilayer structures reveal the fluctuation of C, Si, and N intensities when moving away from the surface, approaching/crossing the C/SiN_x interfaces, and reaching the film/substrate boundary, corroborating well with the actual designs of these multilayer structures. The immediate drop in C intensity and the immediate increase in O intensity in the first 50 s of most of the depth profiles after 5-Mm THW tests indicate that most of the head overcoats had been completely worn off, except in samples C, E, and M. Sample M with just a ~7- to 8-nm-thick overcoat displayed the best wear resistance (about 62% overcoat is still present after 5 Mm of THW) out of all the overcoats used in the present work and even surpasses the wear resistance of previously reported thicker and sputter-deposited ~20- to 100-nm coatings of CrN_x, CrO_x, CN_x, c-BN, yttrium-stabilized ZrO_2, W-C:H, a-C:H, Al_2O_3, and TiN (*13*–*16*).

parameters that need to be tailored according to the scale of tribological measurements. In general, ~2-nm and ~2.5- to 2.75-nm carbon thicknesses (in each layer) and adequate interfacial robustness (based on 4- or 90-eV carbon) are sufficient at the nano- and microscale, respectively, to achieve excellent wear resistance and low friction with C/SiN_x multilayer overcoats. Similarly, ~2.75- to 3-nm carbon thickness and significantly high interfacial robustness/adhesion (based on 350-eV carbon) are required to withstand the wear conditions in a macroscale tribological environment. We elaborate on this here.

The creation of multiple nanoscale interfaces and the tuning of the energy of the arriving carbon ions/atoms in C/SiN_x multilayer designs have led to enhanced atomic intermixing (formation of nanocomposite interfaces) and interfacial bonding, which increased the interfacial strength/robustness between the overcoat and the substrate, thereby contributing to improved adhesion, and also increased the robustness of the overcoat itself. Similarly, the use of high-energy carbon T_1 in carbon superlattice sample E promoted greater atomic mixing and further contributed to the increased adhesion of the overcoat with the substrate. This explains why the carbon superlattice and C/SiN_x multilayer overcoats in certain designs, for example, in samples E, F, G, and M, showed much better nanoscratch resistance than the monolithic carbon overcoats, with sample M being the best performing. Sample F, with a low amount of sp^3 carbon (~2 nm in thickness), showed excellent nanoscratch resistance as well, indicating that increased interfacial robustness/adhesion driven by the introduction of relatively thicker (~1.5 nm) SiN_x layers is the primary parameter for controlling scratch/wear resistance, followed by sp^3 bonding at the nanoscale tribological environment (Fig. 4A). Samples F and G, both of which have ~2-nm carbon layers in multilayer stacks, showed excellent nanoscratch resistance, which suggests that even 2-nm carbon thickness is sufficient at nanoscale to obtain excellent tribological results due to the use of comparably lower measurement loads unlike at the micro- and macrotribological scales.

In the micro- and macroscale tribological environments, low friction can be achieved in both highly sp^3- and highly sp^2-bonded a-C films, thus explaining why samples B, C, and E showed low friction. The low friction in highly sp^2-bonded a-C film (sample B) can primarily be attributed to water intercalation between the sp^2-rich carbon layers and the low shear strength of sp^2 carbon. On the other hand, the low friction in samples C and E is attributed to the combined effects of regular surface passivation of carbon [in an environment with relative humidity (RH) of ~55%], a sufficient initial degree of sp^2 carbon bonding at the surface, and the tribo-induced transformation of $sp^3 \rightarrow sp^2$ bonding at the tribological interface during the test (*4*, *6*, *29*–*33*). The slight tribo-induced increase in sp^2 bonding was confirmed in our sp^3-rich carbon-based films (see Supplementary Discussion 11). Since dangling bonds in carbon induce higher adhesion forces at the tribo interface, the regular passivation of dangling bonds by functional moieties such as C–H, C–OH, C–O, C=O, etc. (*32*) is achieved because of the regular supply of water vapor in a ~55% RH environment, and its continuous dissociation by contact stress and sliding contributes to the lowering of the COF or maintaining it at a constant level. Furthermore, the COF was more stable and lower in the FCVA-processed carbon films, which also yielded better wear resistance due to the presence of higher sp^3 carbon bonding. Among the three samples B, C, and E, the relatively higher friction in monolithic sputtered carbon (sample B) can be attributed to the increased wear of the coating and eventual exposure of the underlying substrate surface to the counterface ball, which was confirmed by Raman spectroscopy analysis on the wear track.

The C/SiN_x multilayer structures demonstrated mixed behaviors in friction and wear. Unlike their nanoscale scratch resistance, samples F and G exhibited the worst microscale tribological properties in terms of very high friction and severe wear. Here, the tribological effect of SiN_x, which itself is a poor tribological material, dominated over the carbon microstructure (sp^3/sp^2 bonding) and interfacial bonding, mainly because of an insufficient carbon thickness to withstand against the counterface at this scale. This was confirmed by the observation of improved tribological properties in both samples K and L where the carbon thickness was increased to 2.75 nm per layer (while the SiN_x layer thickness was reduced accordingly). Moreover, adding high-energy carbon treatment led to the best microscale tribological properties in sample M due to increased atomic intermingling. Thus, we discovered that, for microscale tribology, carbon thickness plays a critical role in realizing superior tribological properties in C/SiN_x multilayer systems. Upon reaching/crossing the critical thickness of carbon (~2.5 to 2.75 nm), the multiple nanoscale interfaces not only enhance the robustness of the film-surface interface but also provide additional bonding strength within the film. These contribute to the improved abilities of overcoats to withstand high contact pressures (*31*, *34*, *35*) during sliding. This explains why the films with inferior interfacial robustness, such as sample B, do not easily survive the high loads applied by the counterface and are eventually worn off during the measurement. On the other hand, both low sp^3-bonded (sample K) and high sp^3-bonded (samples L and M) carbon-based overcoats showed higher wear resistance and lower friction than monolithic carbon; the interfacial robustness effect was found to be relatively more pronounced for carbon with higher sp^3 bonding owing to its higher intrinsic strength. Furthermore, besides the aforementioned factors for low friction in these overcoats, the C/SiN_x multilayer samples with high wear resistance could also contribute to low friction as a result of reduction of wear (*4*, *36*), formation of nanocomposite interfaces due to extensive atomic mixing (C, Si, N, O, Al, and Ti) (*1*, *37*, *38*), and inclusion of Si/Si–O bonds (*39*, *40*) in the carbon network.

When discussing the conditions for a harsh macroscale test environment (such as in THW tests), even the C/SiN_x multilayer overcoat designs in samples K and L failed to provide good wear durability. The poor macroscale wear resistance in sample K is attributed to both the presence of low sp^3 bonding and insufficient interfacial robustness. We recall that sample L with high sp^3 bonding and engineered interfaces based on 90-eV carbon showed excellent tribological behavior in both nanoscale and microscale tribological environments. However, its poor wear resistance in the macroscale tribological environment of the THW test can be mainly attributed to insufficient interfacial robustness needed at this scale. Thus, while keeping the sp^3 bonding and carbon thickness (based on 90-eV carbon) similar to that of sample L, when highly mixed interfaces were created by applying high-energy carbon treatment at 350 eV, which at the same time slightly increased the amount of carbon added to the overall stack, extraordinary macroscale wear durability was realized in sample M. This suggests that the combination of significantly higher interfacial robustness, sufficiently high sp^3 bonding, and a suitable thickness of carbon (~2.75 to 3 nm) and SiN_x are all critical and necessary parameters to obtain high wear durability/wear resistance in a rigorous macroscale tribological environment.

CONCLUSION

We have demonstrated how the degree of atomic intermixing and precise tailoring of nanoscale interfaces in ~7- to 8-nm-thick C/SiN_x multilayer overcoat structures serve to influence their friction and wear engineering at all measurement scales. It was shown that wear and friction engineering of these ultrathin overcoats can be carried out by altering the thicknesses of the individual carbon and SiN_x layers, performing high-energy carbon treatment, and tuning the carbon microstructure. We propose that high interfacial robustness, high adhesion of the overcoat, high sp^3 bonding, and optimal carbon/SiN_x thicknesses are critical parameters to realize high wear resistance and low friction with ultrathin overcoats. On the basis of extensive data, we also conclude that the preference of these critical parameters is highly dependent on the tribological scales: For nanoscale tribological tests, the adhesion of the overcoats (achieved by using a higher SiN_x thickness of ~1.5 nm) is preferred over sp^3 bonding in general, and a carbon thickness of ~2 nm in a C/SiN_x multilayer is sufficient to attain good scratch resistance. In microscale tribological tests, sufficient carbon thickness (~2.5 to 2.75 nm) is a critical parameter, followed by adhesion and sp^3 bonding. In macroscale tests, extremely high adhesion (based on a 350-eV carbon treatment), sufficient carbon thickness (~2.75 to 3.0 nm), and sufficiently high sp^3 bonding are all equally important parameters to obtain high wear durability. The C/SiN_x multilayer overcoat design of 2(0.7SiN_x/T_4/2.75CF) (sample M), which comprised sufficient carbon thickness (~2.75 nm in each layer), lower SiN_x thickness (~0.7 nm in each layer), and a high-energy (350 eV) carbon pretreatment step, turned out to be the exceptional design that yielded excellent wear resistance/wear durability and low friction in tribological tests performed at all three tribological length scales: nano-, micro-, and macroscales. These important findings could aid the development of future ultrathin (<10 nm) overcoats having both super-high wear resistance and low friction that can be applied in advanced MMSDs at all length scales.

MATERIALS AND METHODS

Monolithic carbon, monolithic SiN_x, carbon superlattice, and C/SiN_x multilayer structures were deposited on plasma-cleaned flat AlTiC substrates, commercial magnetic tape head substrates, and flat Si substrates. Monolithic carbon and the carbon layers in the C/SiN_x multilayer structures were deposited by either a low energetic process of pulsed direct current (dc) magnetron sputtering (AJA Inc.) or a high energetic process of FCVA (PVD75 system, which has both FCVA and magnetron sputtering capabilities; Kurt J. Lesker Company, USA), both situated in a class 10 K cleanroom. For all C/SiN_x multilayer structures, the SiN_x layers were deposited by magnetron sputtering in situ with carbon deposition. During the deposition of the FCVA-processed overcoats, the base pressure of the PVD75 system was kept at ~5×10^{-8} torr. The carbon films by FCVA were deposited at a C^+ ion energy of 90 eV. In some samples, a high-energy carbon treatment (T_n) was also performed at a C^+ ion energy of 350 eV. The SiN_x layers in these C/SiN_x multilayer structures were deposited at a radio frequency (rf) power of 60 W and a working pressure of 3 mtorr. The deposition time was adjusted to tune the thicknesses of the SiN_x and carbon layers. On the basis of the treatment time, four different types of high-energy carbon treatments, namely, T_1, T_2, T_3, and T_4, were performed. The times for T_2, T_3, and T_4 were adjusted in such a way that they could contribute to <1-, <0.3-, and <0.5-nm thicknesses, respectively, to the total overcoat thickness. On the other hand, T_1 was performed to intentionally get a thickness of 1.5 nm at 350 eV so as to construct the carbon superlattice sample E [2(T_1/2CF)]. For the sputter-processed overcoats, the monolithic carbon and carbon layers in the C/SiN_x multilayer structures, as well as the SiN_x layers, were deposited in the AJA system using computer-controlled magnetron sputtering. The base pressure was kept at ~7×10^{-9} torr during the deposition. The carbon films were deposited at a working pressure of 5 mtorr and an Ar flow rate of 20 sccm, while 100 W of dc power pulsed at a frequency of 150 kHz and a duty cycle of ~ 40% was supplied to the target. The SiN_x layers in these C/SiN_x multilayer structures were deposited at a working pressure of 3 mtorr and rf power of 120 W. The deposition time was adjusted to tune the thicknesses of the SiN_x and carbon layers, respectively. A detailed discussion on the fabrication of these overcoats can be found in Supplementary Discussions 1 and 2 and (*28*).

The overcoats deposited on flat AlTiC substrates were used for the characterization of interfacial, structural, and functional properties. The overcoats deposited on commercial tape heads were used for the THW tests. The overcoats deposited on Si substrates were used for thickness measurements by HRTEM (Philips CM200). Raman analyses were carried out using a Jobin Yvon LabRAM-HR setup. XPS spectra were recorded using a monochromatic Al K_α source (1486.6 eV) in a VG ESCALAB 220I-XL tool. AFM measurements were performed using a Bruker Innova setup to measure the surface roughness (R_q and R_a) of these overcoats. Nanoindentation measurements were carried out using a Hysitron TI 950 tool with a diamond Berkovich indenter, while nanotribological tests were performed in a Hysitron TI Premier setup to measure the nanomechanical properties (H and E), nanoscale COF, and nanoscratch resistance of the films. A quasi-static partial unload method was used to measure H and E as a function of indentation penetration depth (*9*). Given the ultralow thicknesses of these coatings, it was extremely difficult to avoid the substrate influence on the H and E values of the coatings. Therefore, we compared the H and E results extracted at a fixed penetration depth of ~7 to 8 nm for all samples, which normalizes the substrate influence for all coatings (*9*). Ramping force nanoscratch measurements were carried out to assess the overcoats' scratch resistance through estimating CNF and CNP, indicating the onset of the first failure/delamination event. Microscale tribological measurements were carried out using a ball-on-disk nanotribometer (CSM Instruments) in a cleanroom booth (temperature of 23° ± 1°C and RH of 55 ± 5%), and a sapphire ball (Al_2O_3) with a diameter of 2.0 ± 0.1 mm was used as the counterface. The initial mean and maximum Hertzian contact pressures for Al_2O_3-AlTiC contacts were estimated to be 0.32 and 0.48 GPa, respectively. AES imaging and depth profiles were recorded using a JEOL JAMP Auger Microprobe tool. Long-term THW tests were carried out up to 5 Mm in a custom-made tool to examine the wear durabilities of overcoated heads. It is important to mention that previous overcoats that have been applied onto the tape head, namely, CrN_x, CrO_x, nitrogenated carbon (CN_x), cubic boron nitride (c-BN), yttrium-stabilized ZrO_2 (Y-ZrO_2), hydrogenated amorphous carbon (a-C:H), tungsten incorporated C:H (W-C:H), diamond-like carbon (DLC), Al_2O_3, and titanium nitride (TiN), were very thick (~20 to 100 nm), and most of them suffered from early failure, although the a-C or DLC films fabricated by energetic processes yielded relatively better wear durabilities of all (*12*–*19*). During the tests, the overcoats deposited on LTO-5 tape heads were all tested against LTO-6 barium ferrite

(BaFe) tape, with one tape cartridge being used in each test for the whole 5-Mm test duration. At certain intervals, the head wear (macroscale wear) was analyzed using a combination of optical microscopy (visual observation) and AES. Last, after 5 Mm of THW testing, AES depth profiles were performed on the unworn and worn regions of each tape head to estimate the extent of overcoat removal. For a comprehensive description of sample characterizations, see Supplementary Discussion 2.

SUPPLEMENTARY MATERIALS

Supplementary material for this article is available at http://advances.sciencemag.org/cgi/content/full/5/1/eaau7886/DC1

Supplementary Discussion 1. List of samples and their nomenclature.
Supplementary Discussion 2. Sample preparation and characterization.
Supplementary Discussion 3. HRTEM results and analysis.
Supplementary Discussion 4. TRIM calculations results and analysis.
Supplementary Discussion 5. XPS spectra at various depths and consideration of various effects during analysis.
Supplementary Discussion 6. XPS results and analysis for chemical and interfacial bonding.
Supplementary Discussion 7. Structural properties by XPS and Raman spectroscopy.
Supplementary Discussion 8. Surface roughness of the auxiliary samples.
Supplementary Discussion 9. Nanomechanical and nanotribological properties results and analysis.
Supplementary Discussion 10. Ball-on-disk microscale tribological results and analysis.
Supplementary Discussion 11. Wear track analysis by Raman spectroscopy.
Supplementary Discussion 12. Fundamentals of TD technology and tape heads and evaluation of THW by optical microscopy, AES imaging, and AES depth profiles.
Table S1. Description and nomenclature of all samples.
Fig. S1. HRTEM imaging.
Fig. S2A. TRIM calculations.
Fig. S2B. TRIM calculations.
Fig. S2C. TRIM calculations.
Fig. S2D. TRIM calculations.
Fig. S2E. TRIM calculations.
Fig. S2F. TRIM calculations.
Fig. S2G. TRIM calculations.
Fig. S2H. TRIM calculations.
Fig. S3. XPS analysis.
Fig. S4. Interface analysis by XPS.
Fig. S5. Structural properties.
Fig. S6. Surface roughness measurements of the auxiliary samples.
Fig. S7. AFM imaging before and after nanoindentation and nanoscratch tests.
Fig. S8. Comprehensive friction and wear results for all samples.
Fig. S9. Raman spectroscopy for wear analysis of various samples.
Fig. S10. Fundamentals of magnetic tape heads and analyses of THW by optical microscopy, AES imaging, and AES depth profiles.
References (*41*–*52*)

REFERENCES AND NOTES

1. A. Erdemir, G. Ramirez, O. L. Eryilmaz, B. Narayanan, Y. Liao, G. Kamath, S. K. R. S. Sankaranarayanan, Carbon-based tribofilms from lubricating oils. *Nature* **536**, 67–71 (2016).
2. D. Berman, S. A. Deshmukh, S. K. R. S. Sankaranarayanan, A. Erdemir, A. V. Sumant, Macroscale superlubricity enabled by graphene nanoscroll formation. *Science* **348**, 1118–1122 (2015).
3. H. Bhaskaran, B. Gotsmann, A. Sebastian, U. Drechsler, M. A. Lantz, M. Despont, P. Jaroenapibal, R. W. Carpick, Y. Chen, K. Sridharan, Ultralow nanoscale wear through atom-by-atom attrition in silicon-containing diamond-like carbon. *Nat. Nanotechnol.* **5**, 181–185 (2010).
4. N. Dwivedi, R. J. Yeo, Z. Zhang, C. Dhand, S. Tripathy, C. S. Bhatia, Interface engineering and controlling the friction and wear of ultrathin carbon films: High sp^3 versus high sp^2 carbons. *Adv. Funct. Mater.* **26**, 1526–1542 (2016).
5. M. Palacio, B. Bhushan, Ultrathin wear-resistant ionic liquid films for novel MEMS/NEMS applications. *Adv. Mater.* **20**, 1194–1198 (2008).
6. N. Dwivedi, R. J. Yeo, L. J. K. Yak, N. Satyanarayana, C. Dhand, T. N. Bhat, Z. Zhang, S. Tripathy, C. S. Bhatia, Atomic scale interface manipulation, structural engineering, and their impact on ultrathin carbon films in controlling wear, friction, and corrosion. *ACS Appl. Mater. Interfaces* **8**, 17606–17621 (2016).
7. M. A. Lantz, B. Gotsmann, P. Jaroenapibal, T. D. B. Jacobs, S. D. O'Connor, K. Sridharan, R. W. Carpick, Wear-resistant nanoscale silicon carbide tips for scanning probe applications. *Adv. Funct. Mater.* **22**, 1639–1645 (2012).
8. E. Rismani, S. K. Sinha, S. Tripathy, H. Yang, C. S. Bhatia, Effect of pre-treatment of the substrate surface by energetic C^+ion bombardment on structure and nano-tribological characteristics of ultra-thin tetrahedral amorphous carbon (ta-C) protective coatings. *J. Phys. D Appl. Phys.* **44**, 115502 (2011).
9. R. J. Yeo, N. Dwivedi, L. Zhang, Z. Zhang, C. Y. H. Lim, S. Tripathy, C. S. Bhatia, Superior wear resistance and low friction in hybrid ultrathin silicon nitride/carbon films: Synergy of the interfacial chemistry and carbon microstructure. *Nanoscale* **9**, 14937–14951 (2017).
10. R. J. Yeo, N. Dwivedi, E. Rismani, N. Satyanarayana, S. Kundu, P. S. Goohpattader, H. R. Tan, N. Srinivasan, B. Druz, S. Tripathy, C. S. Bhatia, Enhanced tribological, corrosion, and microstructural properties of an ultrathin (<2 nm) silicon nitride/carbon bilayer overcoat for high density magnetic storage. *ACS Appl. Mater. Interfaces* **6**, 9376–9385 (2014).
11. F. Rose, D. Pocker, Q.-F. Xiao, V. Rawat, E. Brinkman, B. Marchon, Low surface energy and corrosion resistant ultrathin TiSiC disk overcoat. *J. Appl. Phys.* **113**, 213513 (2013).
12. R. J. Yeo, N. Dwivedi, L. Zhang, Z. Zhang, C. Y. H. Lim, S. Tripathy, C. S. Bhatia, Durable ultrathin silicon nitride/carbon bilayer overcoats for magnetic heads: The role of enhanced interfacial bonding. *J. Appl. Phys.* **117**, 045310 (2015).
13. B. Bhushan, G. S. A. M. Theunissen, X. Li, Tribological studies of chromium oxide films for magnetic recording applications. *Thin Solid Films* **311**, 67–80 (1997).
14. E. Sourty, J. L. Sullivan, M. D. Bijker, Chromium oxide coatings applied to magnetic tape heads for improved wear resistance. *Tribol. Int.* **36**, 389–396 (2003).
15. G. S. A. M. Theunissen, Wear coatings for magnetic thin film magnetic recording heads. *Tribol. Int.* **31**, 519–523 (1998).
16. P. K. Bachmann, H. Lade, D. Leers, D. U. Wiechert, G. S. A. M. Theunissen, Wear testing of CVD diamond films. *Diamond Relat. Mater.* **3**, 799–804 (1994).
17. B. Shi, J. L. Sullivan, S. O. Saied, A study of thin coating wear in high data density tape heads. *J. ASTM Int.* **5**, JAI101192 (2008).
18. W. W. Scott, B. Bhushan, A. V. Lakshmikumaran, Ultrathin diamond-like carbon coatings used for reduction of pole tip recession in magnetic tape heads. *J. Appl. Phys.* **87**, 6182–6184 (2000).
19. B. Bhushan, B. K. Gupta, R. Sundaram, S. Dey, S. Anders, A. Anders, I. G. Brown, P. D. Reader, Development of hard carbon coatings for thin-film tape heads. *IEEE Trans. Magn.* **31**, 2976–2978 (1995).
20. C. Casiraghi, A. C. Ferrari, R. Ohr, D. Chu, J. Robertson, Surface properties of ultra-thin tetrahedral amorphous carbon films for magnetic storage technology. *Diamond Relat. Mater.* **13**, 1416–1421 (2004).
21. C. Casiraghi, J. Robertson, A. C. Ferrari, Diamond-like carbon for data and beer storage. *Mater. Today* **10**, 44–53 (2007).
22. J. Robertson, Requirements of ultrathin carbon coatings for magnetic storage technology. *Tribol. Int.* **36**, 405–415 (2003).
23. A. Anders, W. Fong, A. V. Kulkarni, F. W. Ryan, C. S. Bhatia, Ultrathin diamond-like carbon films deposited by filtered carbon vacuum arcs. *IEEE Trans. Plasma Sci.* **29**, 768–775 (2001).
24. A. A. Balandin, M. Shamsa, W. L. Liu, C. Casiraghi, A. C. Ferrari, Thermal conductivity of ultrathin tetrahedral amorphous carbon films. *Appl. Phys. Lett.* **93**, 043115 (2008).
25. A. C. Ferrari, J. Robertson, Resonant Raman spectroscopy of disordered, amorphous, and diamondlike carbon. *Phys. Rev. B* **64**, 075414 (2001).
26. J. F. Ziegler, J. P, Biersack, U. Littmark, *The Stopping and Range of Ions in Solids*, vol. 1 of *Stopping and Ranges of Ions in Matter* (Pergamon Press, 1984).
27. H.-C. Tsai, D. B. Bogy, Characterization of diamondlike carbon films and their application as overcoats on thin-film media for magnetic recording. *J. Vac. Sci. Technol. A* **5**, 3287–3312 (1987).
28. N. Dwivedi, R. J. Yeo, Z. Zhang, C. Dhand, S. Tripathy, C. S. Bhatia, Direct observation of thickness and foreign interlayer driven abrupt structural transformation in ultrathin carbon and hybrid silicon nitride/carbon films. *Carbon* **115**, 701–719 (2017).
29. A. Erdemir, C. Donnet, Tribology of diamond-like carbon films: Recent progress and future prospects. *J. Phys. D Appl. Phys.* **39**, R311–R327 (2006).
30. T. Kunze, M. Posselt, S. Gemming, G. Seifert, A. R. Konicek, R. W. Carpick, L. Pastewka, M. Moseler, Wear, plasticity, and rehybridization in tetrahedral amorphous carbon. *Tribol. Lett.* **53**, 119–126 (2014).
31. H. Ronkainen, K. Holmberg, in *Tribology of Diamond-like Carbon Films: Fundamentals and Applications*, C. Donnet, A. Erdemir, Eds. (Springer, 2008), chap. 6.
32. A. R. Konicek, D. S. Grierson, A. V. Sumant, T. A. Friedmann, J. P. Sullivan, P. U. P. A. Gilbert, W. G. Sawyer, R. W. Carpick, Influence of surface passivation on the friction and wear behavior of ultrananocrystalline diamond and tetrahedral amorphous carbon thin films. *Phys. Rev. B* **85**, 155448 (2012).
33. T. W. Scharf, I. L. Singer, Role of the transfer film on the friction and wear of metal carbide reinforced amorphous carbon coatings during run-in. *Tribol. Lett.* **36**, 43–53 (2009).
34. T. C. O'Sullivan, R. B. King, Sliding contact stress field due to a spherical indenter on a layered elastic half-space. *J. Tribol.* **110**, 235–240 (1988).

35. S. Ramalingam, L. Zheng, Film-substrate interface stresses and their role in the tribological performance of surface coatings. *Tribol. Int.* **28**, 145–161 (1995).
36. N. W. Khun, E. Liu, Influence of carbon sputtering power on structure, corrosion resistance, adhesion strength and wear resistance of platinum/ruthenium/nitrogen doped diamond-like carbon thin films. *Surf. Coat. Technol.* **205**, 853–860 (2010).
37. O. Wilhelmsson, M. Råsander, M. Carlsson, E. Lewin, B. Sanyal, U. Wiklund, O. Eriksson, U. Jansson, Design of nanocomposite low-friction coatings. *Adv. Funct. Mater.* **17**, 1611–1616 (2007).
38. A. A. Voevodin, J. P. O'Neill, J. S. Zabinski, Nanocomposite tribological coatings for aerospace applications. *Surf. Coat. Technol.* **116–119**, 36–45 (1999).
39. J. Lanigan, H. Zhao, A. Morina, A. Neville, Tribochemistry of silicon and oxygen doped, hydrogenated diamond-like carbon in fully-formulated oil against low additive oil. *Tribol. Int.* **82**, 431–442 (2015).
40. K. D. Koshigan, F. Mangolini, J. B. McClimon, B. Vacher, S. Bec, R. W. Carpick, J. Fontaine, Understanding the hydrogen and oxygen gas pressure dependence of the tribological properties of silicon oxide–doped hydrogenated amorphous carbon coatings. *Carbon* **93**, 851–860 (2015).
41. W. C. Oliver, G. M. Pharr, An improved technique for determining hardness and elastic modulus using load and displacement sensing indentation experiments. *J. Mater. Res.* **7**, 1564–1583 (1992).
42. P. Reinke, G. Francz, O. Oelhafen, J. Ullmann, Structural changes in diamond and amorphous carbon induced by low-energy ion irradiation. *Phys. Rev. B* **54**, 7067–7073 (1996).
43. N. S. McIntyre, H. Y. Nie, A. P. Grosvenor, R. D. Davidson, D. Briggs, XPS studies of octadecylphosphonic acid (OPA) monolayer interactions with some metal and mineral surfaces. *Surf. Interface Anal.* **37**, 749–754 (2005).
44. R. Haerle, E. Riedo, A. Pasquarello, A. Baldereschi, Sp2/sp3 hybridization ratio in amorphous carbon from C 1s core-level shifts: X-ray photoelectron spectroscopy and first-principles calculation. *Phys. Rev. B* **65**, 045101 (2001).
45. E. Rismani, S. K. Sinha, H. Yang, C. S. Bhatia, Effect of pretreatment of Si interlayer by energetic C^+ ions on the improved nanotribological properties of magnetic head overcoat. *J. Appl. Phys.* **111**, 084902 (2012).
46. P. Bunnak, Y. Gong, S. Limsuwan, A. Pokaipisit, P. Limsuwan, Chemical bonding in composite SiN_x/diamond-like carbon films prepared by filter cathodic arc deposition of graphite incorporated with radio frequency sputtering of silicon nitride. *Jpn. J. Appl. Phys.* **52**, 095501 (2013).
47. N. Hellgren, J. Guo, Y. Luo, C. Såthe, A. Agui, S. Kashtanov, J. Nordgren, H. Ågren, J.-E. Sundgren, Electronic structure of carbon nitride thin films studied by X-ray spectroscopy techniques. *Thin Solid Films* **471**, 19–34 (2005).
48. R. Bertoncello, A. Casagrande, M. Casarin, A. Glisenti, E. Lanzoni, E. Tondello, TiN, TiC and Ti(C, N) film characterization and its relationship to tribological behaviour. *Surf. Interface Anal.* **18**, 525–531 (1992).
49. A. Schüler, P. Oelhafen, In situ core-level and valence-band photoelectron spectroscopy of reactively sputtered titanium aluminum nitride films. *Phys. Rev. B* **63**, 115413 (2001).
50. I. Strydom, S. Hofmann, The contribution of characteristic energy losses in the core-level X-ray photoelectron spectroscopy peaks of TiN and (Ti, Al)N studied by electron energy loss spectroscopy and X-ray photoelectron spectroscopy. *J. Electron Spectrosc. Relat. Phenom.* **56**, 85–103 (1991).
51. E. Rismani, R. Yeo, S. K. Sinha, H. Yang, C. S. Bhatia, Developing an $(Al,Ti)N_xC_y$ interlayer to improve the durability of the ta-C coating on magnetic recording heads. *Tribol. Lett.* **50**, 233–243 (2013).
52. S.-E. Ong, S. Zhang, H. Du, D. Sun, Relationship between bonding structure and mechanical properties of amorphous carbon containing silicon. *Diamond Relat. Mater.* **16**, 1628–1635 (2007).

Acknowledgments: We thank Z. Lu from the Institute of Microelectronics, A*STAR Singapore and Z. Zhang of the Institute of Materials Research and Engineering, A*STAR Singapore for their help in AES and XPS measurements, respectively. **Funding:** This research was partially supported by the National Research Foundation, Prime Minister's Office, Singapore under its Competitive Research Programme (CRP award no. NRF-CRP 4-2008-06) and the A*STAR Nanoimprint Foundry (project no. 1525300037). A part of this work was performed at the Center for Nanoscale Materials, a U.S. Department of Energy Office of Science User Facility, and supported by the U.S. Department of Energy, Office of Science, under contract no. DE-AC02-06CH11357. **Author contributions:** N.D. and C.S.B. conceived the idea and designed the project. N.D. and R.J.Y. prepared all the samples. N.D., R.J.Y., C.D., J.R., R.N., and S.T. performed characterizations. N.D. and C.D. prepared chemical models. N.D. analyzed most of the results. All authors contributed in analysis of the data. N.D. wrote the initial draft of the manuscript. C.S.B., A.D., H.Y., S.R., M.S.M.S., S.K.R.S.S., and R.J.Y. provided constructive suggestions on the analysis and manuscript draft. All authors critically reviewed the manuscript. **Competing interests:** The authors declare that they have no competing interests. **Data and materials availability:** All data needed to evaluate the conclusions in the paper are present in the paper and/or the Supplementary Materials. Additional data related to this paper may be requested from the authors.

Submitted 16 July 2018
Accepted 6 December 2018
Published 18 January 2019
10.1126/sciadv.aau7886

Citation: N. Dwivedi, R. J. Yeo, C. Dhand, J. Risan, R. Nay, S. Tripathy, S. Rajauria, M. S. M. Saifullah, S. K. R. S. Sankaranarayanan, H. Yang, A. Danner, C. S. Bhatia, Boosting contact sliding and wear protection via atomic intermixing and tailoring of nanoscale interfaces. *Sci. Adv.* **5**, eaau7886 (2019).